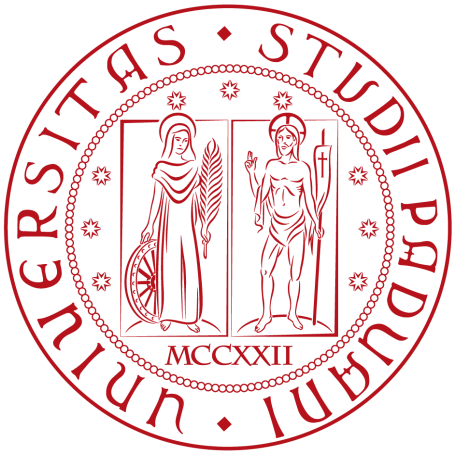

Università degli studi di Padova

Dipartimento di Fisica e Astronomia "Galileo Galilei"
Laurea Triennale in Fisica

Lifetime measurements of excited states in nuclei around the doubly-magic ^{48}Ca and ^{208}Pb

Laureando:
Lorenzo Longo,
1004322

Relatori:
Chia.mo Prof. Santo Lunardi
Dott. J.J. Valiente-Dobòn

Anno accademico 2014–2015

Contents

Chapter 1

Introduction

In this work, the results of two experiments devoted to lifetime measurements of nuclear excited states will be presented.

In the first one, the goal was to measure lifetimes in the picosecond range for the first excited states of ^{50}Ca and ^{51}Sc, which have, respectively, two neutrons and two neutrons-one proton more than the doubly-magic ^{48}Ca, see figure 1.1.

The two nuclei have been populated via a multi-nucleon transfer reaction induced by a ^{48}Ca beam on a ^{208}Pb target.

The lifetime of the 1026-keV (2^+) state of ^{50}Ca, and the 1065-keV $(11/2^-)$ state of ^{51}Sc will be presented. The knowledge of the lifetimes of these states will allow to determine the reduced transition probability and therefore to understand their character in terms of a shell-model description around the double shell-closure Z=20 and N=28.

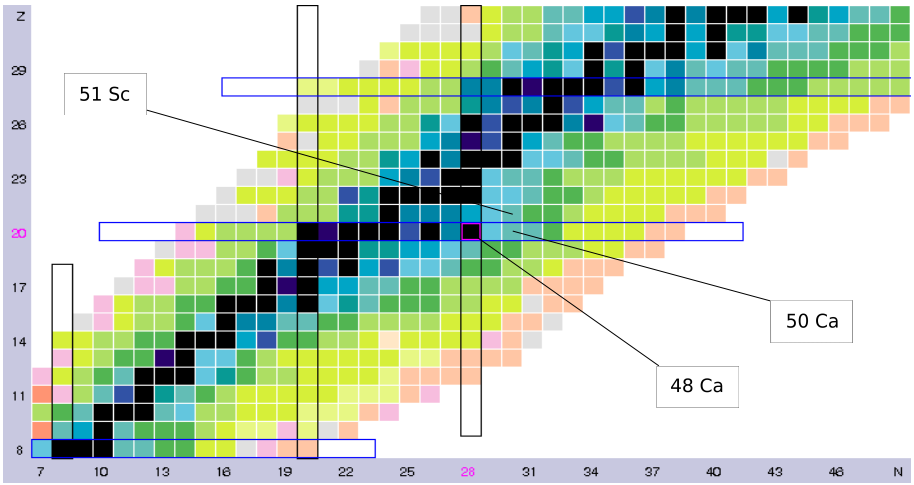

Figure 1.1: Chart of nuclides. Zoom on the region of interest around the doubly magic ^{48}Ca nucleus.

In the second experiment I will discuss the lifetimes of isomeric states in ^{198}Au and ^{202}Pb which are just a few nucleons below the doubly-magic nucleus ^{208}Pb, see figure 1.2.

Isomeric states are charaterized by longer lifetimes, higher than few nanoseconds, depending on the structure of the two energy levels involved in the γ decay. I will discuss in detail the 312-keV (5^+) state of ^{198}Au, and the chain decay of the $5242 + \delta$-keV (19^-) and $4091 + \Delta$-keV (16^+) isomeric states in ^{202}Pb. The excited states in the two nuclei were populated via a multi-nucleon transfer reaction between a ^{82}Se beam and a ^{198}Pt target.

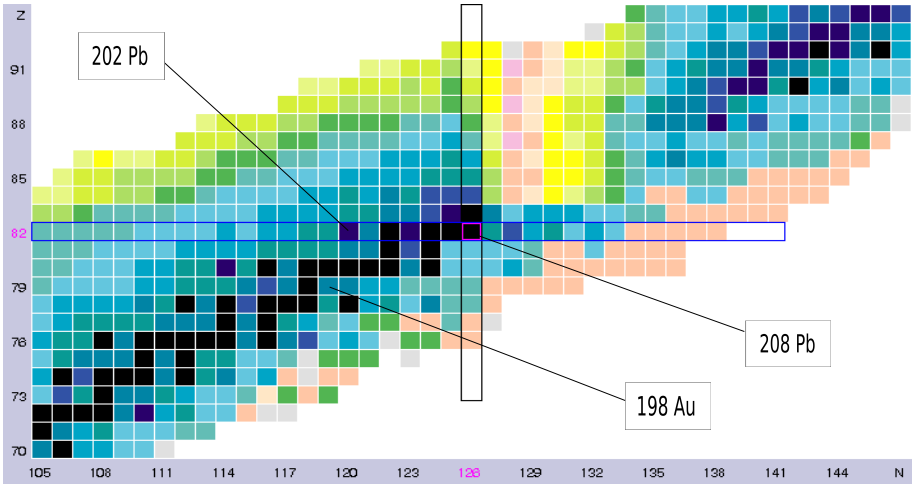

Figure 1.2: Chart of nuclides. Zoom on the region of interest around the doubly magic ^{208}Pb nucleus.

Chapter 2

The CLARA-PRISMA and AGATA-PRISMA set-ups

I will now briefly describe the experimental apparata used in the $^{48}Ca + ^{208}Pb$ and $^{82}Se + ^{198}Pt$ experiments to identify the final nuclei, measure the γ-ray transitions and the lifetimes of their excited states.

2.1 The PRISMA spectrometer

The PRISMA [1] spectrometer is a large acceptance magnetic spectrometer, which has been designed for the identification of the reaction products of binary heavy ions collisions in the energy range of $\approx 5 - 10$ MeV/A.

Figure 2.1 shows the different components described in the following:

- Two optical elements:
  - a quadrupole magnet (A);
  - a dipole magnet (B);
- A system of detectors providing position, energy and Time Of Flight (TOF) information:
  - a Micro-Channel Plate entrance detector (MCP) (C)
  - a Multi-Wire Parallel Plate Avalanche Counter focal plane detector (MWP-PAC) (D)
  - an Ionisation Chamber (IC) (E)

The magnetic spectrometer PRISMA allows to completely identify the reaction products in atomic and mass number (Z and A), and to measure their velocities. The quadrupole and the dipole are used to focus the ions on the vertical axis to the dispersion plane, and to bend the trajectories of the ions to the focal plane detectors. The three main detectors of the spectrometer, the MCP entrance detector, the MWPPAC and the IC at the focal plane, provide

information on the entrance and exit position, on the TOF of the ions (defined as the difference between the time signals given by the MCP and the MWPPAC), on the total and partial kinetic energies deposited in the IC sections, and on the range of the ions in the IC. Through these signals it is possible to derive the trajectories and the velocity of incoming ions.
The characteristics of the spectrometer are:

- large solid angle, approximately $80msr$
- momentum acceptance $\pm 10\%$
- mass resolution up to $\Delta A/A \approx 1/300$ achieved via TOF
- Z resolution $\Delta Z/Z \approx 1/60$ using the IC
- energy resolution up to $1/1000$
- rotation around the target in the angular range $20° \leq \theta \leq 130°$

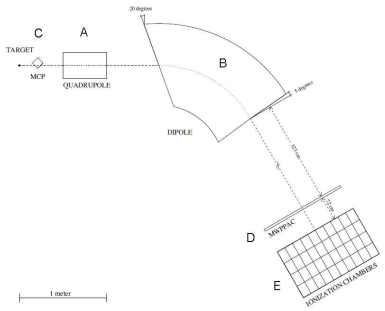

Figure 2.1: On the left a photo of PRISMA. On the right the scheme of the spectrometer. See text for details.

2.2 The CLARA germanium array

The CLARA [2] germanium array is a γ spectrometer composed of 25 clover germanium detectors, see Figure 2.2. The intrinsic energy resolution of the Ge array is 3 keV at 1.3 MeV, while a FWHM of 0.9% is obtained for γ rays released by moving ions at $\approx 10\%$ of the speed of light (that is the typical $\beta = \frac{v}{c}$ of the ions considered in this thesis). The CLARA array surrounds the scattering chamber to form a hemisphere, covering a solid angle of 2π steradians. It has a large granularity, around 100 crystals, and the total photopeak efficiency is $\approx 3\%$ for 1.3 MeV γ rays.

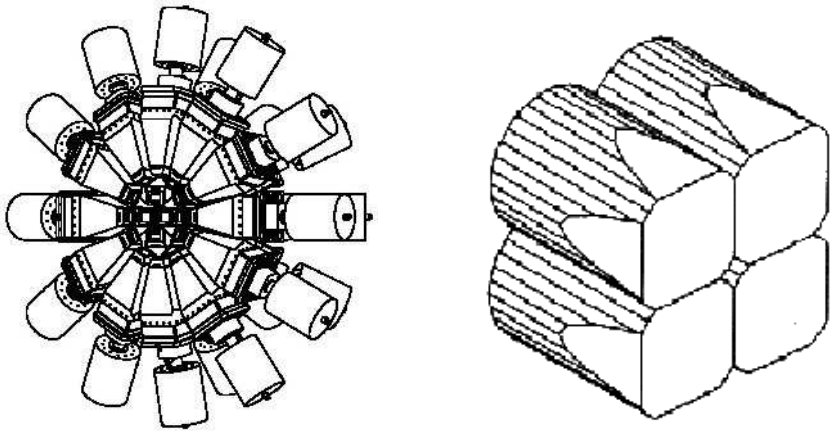

Figure 2.2: A schematic view of CLARA and a single clover detector.

2.3 The Plunger setup

The Plunger [3, 4] is a special target-degrader complex that has been built to measure lifetimes in the picosecond range of excited states in nuclei.

In our case it consists of a target of 1.0 mg/cm^2 of enriched ^{208}Pb evaporated onto a 1.0 mg/cm^2 Thallium support to accomplish the stretching of the target, and of a thick 4.0 mg/cm^2 Magnesium foil, used as an energy degrader. The procedure for stretching simultaneously the target and the degrader foils as well as the dedicated target holder have been developed at the Institute of Nuclear Physics at the University of Köln. The target-degrader distance is a crucial parameter. Different distances, ranging from 100 μm to 2200 μm, were employed during the experiment by arranging a stack of various metallic rings, whose thickness accuracy was better than 1.0 μm. Figure 2.3 shows two pictures of the plunger setup.

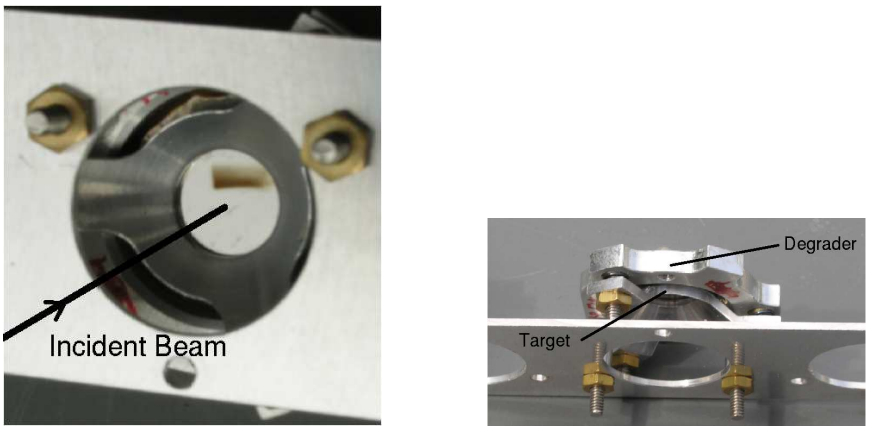

Figure 2.3: The Plunger device from different views [5].

2.4 The AGATA germanium array

The Advanced GAmma Tracking Array (AGATA) [6, 7] is a γ spectrometer based on the novel concepts of pulse shape analysis and γ-ray tracking with highly segmented Ge semiconductor detectors.

The AGATA sub-array being installed at LNL consists of five triple cluster elements (see Fig. 2.4). Given the number of elements, the optimal geometry of the array for the experimental activity at LNL is the compact distribution of the 15 Ge crystals arranged in the mentioned five triple clusters. This sub-array of AGATA is placed symmetrically along the optical axis of the PRISMA spectrometer at approximately 180°. This is the optimal position to minimize the Doppler broadening.

The full AGATA 4π geometry is based on 180 detectors, i.e. 60 AGATA triple clusters. The sub-array of AGATA coupled to the PRISMA spectrometer is placed onto a platform that rotates from 0° to 117° with respect to the beam direction. Both devices are fixed on the platform and are located face-to-face in such a way that, independently of the spectrometer angle selected for an experiment, the recoils that enter into the PRISMA spectrometer will have a trajectory of approximately 180° with respect to the central axis of the AGATA sub-array.

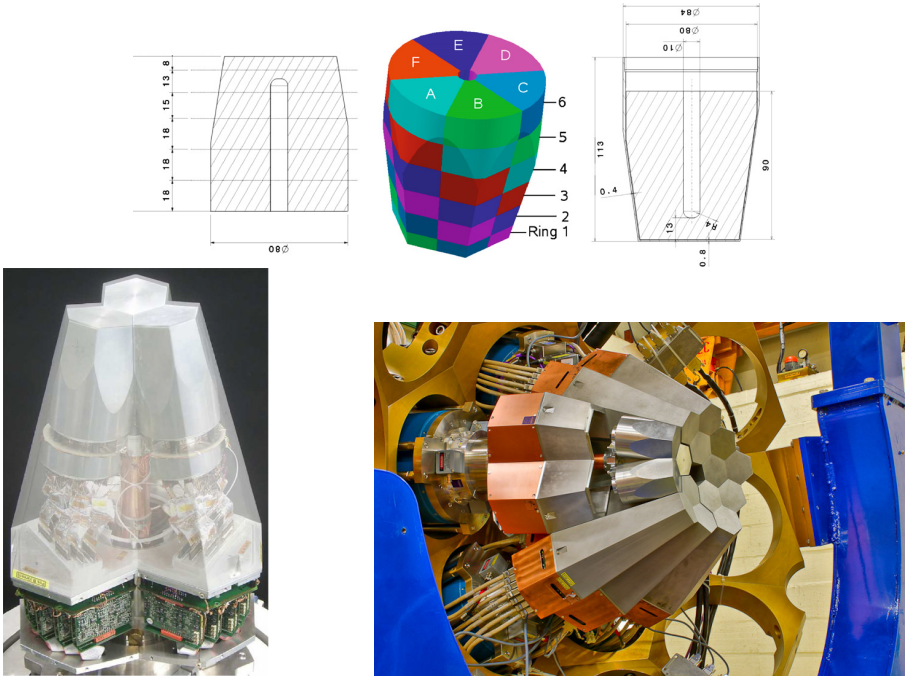

Figure 2.4: On the top: the segmentation of an AGATA detector (left and middle). The dimensions are given in mm. On the right side the encapsulation is drawn. On the bottom: the mounted AGATA triple cluster, with the cryostat (left). On the right a photo of the AGATA demonstrator.

Chapter 3

Lifetime measurements of neutron-rich nuclei around the doubly magic nucleus ^{48}Ca

In this chapter I will discuss the lifetime results obtained for the ^{50}Ca and ^{51}Sc nuclei populated in the $^{48}Ca + ^{208}Pb$ multinucleon-transfer reaction. These nuclei are respectively two neutrons and two neutrons-one proton above the doubly-magic nucleus ^{48}Ca. The knowledge of the lifetimes of the first excited states will allow to understand their character in terms of a shell-model description around the double shell-closure $Z = 20$ and $N = 28$.

I will in the following explain in detail the experimental procedure, the analysis of the data, and eventually discuss the results for the states of interest.

3.1 The $^{48}Ca + ^{208}Pb$ experiment

The apparatus used with the $^{48}Ca + ^{208}Pb$ experiment consists of the magnetic spectrometer PRISMA coupled to the array of germanium detectors CLARA. Inside the scattering chamber the target-degrader system, called Plunger, was mounted. This experimental setup, combining a large acceptance mass spectrometer with a γ-detector array, allows to identify a particular reaction product and to associate to it the γ transitions deexciting its excited states. The Plunger device allows to measure the lifetime of the states of interest which deexcite through γ-ray emission.

3.2 Population of neutron-rich nuclei

The different nuclear reactions between heavy ions possible at the Tandem-ALPI accelerator of Legnaro can be, generally speaking, divided into three main categories, depending on the energy of the beam. Beside the centre-of-mass energy,

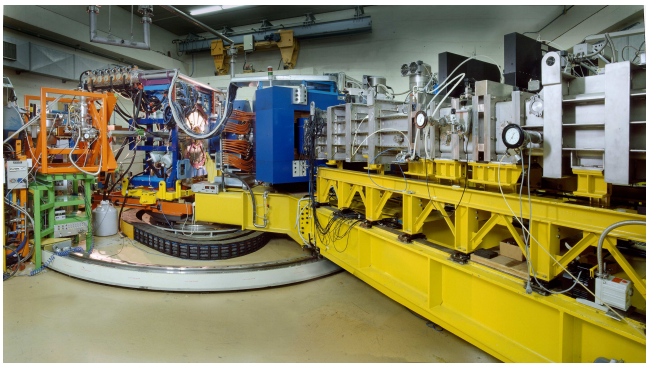

Figure 3.1: A photo of CLARA coupled to the PRISMA spectrometer.

the impact parameter and the nature of the projectile and target are also essential ingredients in defining the type of reaction. The three main reaction mechanisms which occur when two heavy-ions collide are:

inelastic reactions in which the colliding nuclei simply scatter one from the other without exchanging nucleons;

fusion-evaporation reactions characterized by small impact parameter and interacting time of the order of 10^{-16} - 10^{-18} s. In these reactions all the beam energy is converted into excitation of the internal degrees of freedom of the resulting compound nucleus. As a consequence, high-spin states can be populated;

multi-nucleon transfer reactions in which the impact parameter is extended compared to fusion-evaporation reactions, so that the collision is more peripheral, but the interaction time is much shorter (about 10^{-22} s). This method is a powerful tool in order to populate neutron-rich nuclei.

The method that has been used to populate neutron-rich nuclei in our case is in fact a multi-nucleon transfer reaction [8] between an incident beam of ^{48}Ca, at a bombarding energy of 310 MeV, and a ^{208}Pb target [9]. At this energy the two colliding nuclei transfer a certain number of neutrons and protons, in a very short interaction time ($\sim 10^{-22}$ s). The resulting products are called, according to their mass, *Beam-Like Fragments* (BLF) and *Target-Like Fragments* (TLF).

The cross section of the reaction is at its maximum when the BLF are scattered at a certain angle, where one should locate the detector (PRISMA) for ions identification to reach the highest possible statistics. In the laboratory frame this angle (see Fig. 3.2) is called the *grazing angle* (θ_g). Multinucleon-transfer reactions are extremely important, since they allow to populate neutron-rich regions of the nuclide chart that cannot be reached with fusion-evaporation reactions using stable beams and targets.

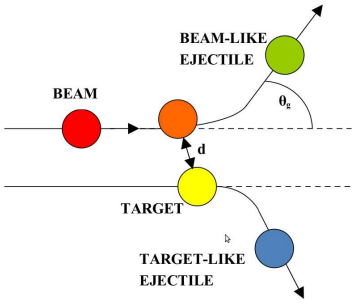

Figure 3.2: Scheme of a binary nuclear reaction. Beam-Like Ejectile and Target-Like Ejectile are the BLF and TLF mentioned in the text above respectively. θ_g is the grazing angle

3.3 Lifetimes measurements: the RDDS method

To measure the lifetimes of nuclear excited states in the picosecond range the major tool is the Recoil Distance Doppler Shift method (RDDS) [3, 10]. It consists in placing, after the target, an energy degrader at variable distances, and to measure, as function of such distance, the γ rays emitted by the excited states of the recoiling ions whose mass and atomic number is measured in a spectrometer.

Depending whether a γ ray, de-exciting a particular state, is emitted before or after the degrader, it exhibits different Doppler shifts (see next section). Therefore, for each transition, the γ spectrum shows two peaks. The higher-energy one, E'_γ, corresponds to γ rays emitted after passing the degrader, with an average velocity of $\beta' \approx 8.0\%$. The lower-energy one, E_γ, corresponds to γ rays emitted before the degrader, with an average velocity of $\beta \approx 10.0\%$. The relative intensities of the peak areas as a function of the target-degrader distance determine the lifetime of the state of interest.

3.3.1 The Doppler correction

As described above, in this experiment γ rays are emitted from sources at two different velocities, and therefore a proper Doppler correction allows us to distinguish between decays occurring before and after the degrader. The Doppler effect occurs when light, or another wave, is emitted from a source in relative motion with respect to the observer. It is similar to the well known effect of sound waves. However for the light this effect has different consequences due to the relation $E = h\nu$ and to the special relativity. When the source of a photon (in our case an ion emitting a γ ray) is moving with $\beta = v/c$ and the observer (a single detector of CLARA, described on section 3.2) measures a photon emitted with an angle θ (extimated on section 4.1) with respect to the ion velocity vector $\overrightarrow{\beta}$, the frequency measured from the observer (ν_0) is different from the frequency of the emitted photon in its frame of reference (ν_s). The general equation, that relates the energies in the two different reference frames is [11]:

$$\nu_s = \nu_0[(1-\beta^2)^{1/2}(1+\beta cos\theta)]$$

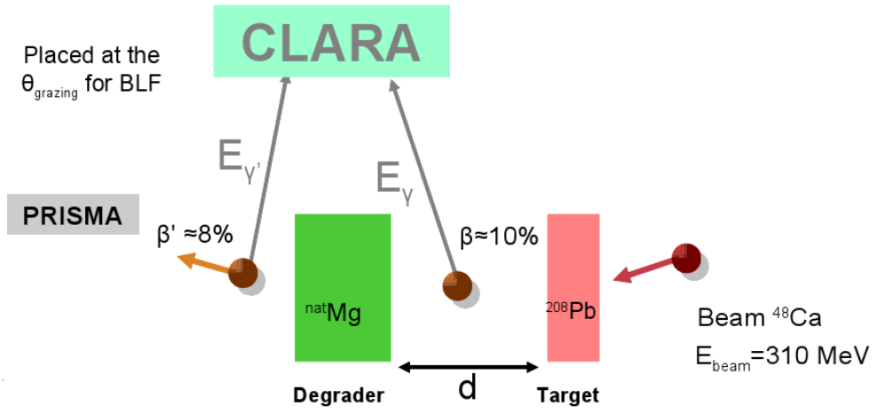

Figure 3.3: Schematic drawing of the experimental apparatus for lifetime measurements. BLF represents the Beam-Like Fragments entering PRISMA, d the target-degrader distance. β and β' are the velocities of excited nuclei before and after the degrader respectively, E_γ and E_γ' are the energies of the Doppler-corrected γ-rays emitted before and after the degrader respectively.

For the case studied in this thesis, typical β values are $\approx 10\%$, and we can apply the approximation $\beta \ll 1$. Therefore, considering only the first Taylor terms we obtain:

$$\nu_s = \nu_0(1 + \beta cos\theta)$$

and the observer (CLARA) detects the photon with an energy different from the energy of the same photon in the rest frame of reference. The measured energy of the photon is:

$$E_s = E_\gamma = E_0(1 + \beta cos\theta) \tag{3.1}$$

3.3.2 The velocity of the recoiling ions

The experimental setup used in this experiment, described in chapter 2 and in section 3.1, allows to measure γ spectra in the frame of reference of the laboratory and at the same time the velocity of the excited ions that decay by emitting γ rays. The relations between the true energy of the γ rays, measured when emitted before and after the degrader (E_γ and E'_γ), in the approximation $\beta \ll 1$ are:

$$E_\gamma = E_0(1 + \beta cos\theta) \tag{3.2}$$

$$E'_\gamma = E_0(1 + \beta' cos\theta) \tag{3.3}$$

With the PRISMA spectrometer it is possible to measure the distribution of β' (shown in Fig.s 3.5(c) and 3.6(c)) of the ions that have passed the degrader and entered PRISMA. The Doppler correction is therefore the right one for ions that decay after the degrader (eq. 2.3), and in fact the corresponding γ rays appear on the γ spectra with the correct energy value, whereas it gives a wrong

value of E_0 for ions decayed before the degrader. The wrongly-corrected γ rays appear on the γ spectra as a shifted peak, with the energy:

$$E_0^{shifted} = E_\gamma(1 - \beta cos\theta)$$

Substituting E_γ with the equation 3.1 and re-arranging the resulting equation, it is possible to obtain a relation that allows to calculate β, since all the other variables are known:

$$\frac{E_0 - E_0^{shifted}}{E_0} = (\beta' - \beta)cos\theta \tag{3.4}$$

3.4 The radioactive decay of excited nuclei

The radioactive decay is a probabilistic process [12]. The total production of parent excited states depends on the rate of production and on the total lenght of the experiment, and it is equal to $N_1(0)$. So it is possible to express the law of a single decay with the differential relation 3.5, where λ is the decay probability and $\frac{1}{\lambda} = \tau$ is the lifetime:

$$dN_1 = -\lambda_1 N_1 dt \tag{3.5}$$

One obtains then the classical exponential law:

$$N_1(t) = N_0 e^{-\lambda_1 t} \tag{3.6}$$

It is then useful to define the *lifetime* τ of the sample as the reverse of the decay constant:

$$\tau = \frac{1}{\lambda}$$

The measurement of the *lifetime* τ of some excited states is the purpose of the experiment described in this chapter.

3.4.1 Lifetime measurement for a simple exponential decay

Gating on a specific mass number A and on the atomic number Z measured by the PRISMA spectrometer one obtains the γ spectrum associated to the decay of its excited states. In our analysis we will compare the γ-ray spectra obtained at different target-degrader distances and extract from each of them the areas of the γ ray of interest emitted before and after the degrader.
Knowing the target-degrader distance (d) and the true velocity of the ions (β), calculated as explained in the previous section, one can express the number of decays after the degrader (un-shifted, eq. 1.9), and those before (shifted, eq. 1.10) through the relations:

$$I_u(t) = N_0 e^{-\frac{d}{v\tau}} \tag{3.7}$$

$$I_s(t) = N_0 - N_0 e^{-\frac{d}{v\tau}} \tag{3.8}$$

where I_u and I_s are the areas of the unshifted and shifted peaks, respectively. These areas are obtained with a simple integral of the peak, which has been fitted through a gaussian fit after having subtracted the background. In order to obtain a result indipendent from the effective number of radioactive nuclei produced within the reaction, we consider the *Ratio* defined as:

$$R = \frac{I_u}{I_u + I_s} = e^{-\frac{d}{v\tau}} = e^{-\frac{d}{\beta c\tau}} \tag{3.9}$$

Then, by fitting an exponential function (see Ref. [2]) for R (or a linear regression for the linearized function $-lnR(d) = \frac{d}{\beta c\tau}$) as function of distance d, it is possible to extract the lifetime τ of the excited states.

3.5 Experimental details

The Plunger device has been placed in the geometrical center of the reaction chamber of the CLARA-PRISMA setup, as it is shown in Fig. 3.4. Due to mechanical constraints, it could not be placed perpendicular to the optical axis of the spectrometer, but at an angle of 22° with respect to the beam. In this experiment PRISMA was placed at 49° with respect to the incident beam, the *grazing angle* of the reaction. The thickness of the degrader is $d_{deg} \approx 23\mu m$, but, due to the angle of 27° between the degrader and the optical axis of PRISMA, the effective thickness experienced by ions is of $d_{deg}/cos\ 27°$. Therefore, the true distance travelled by the ions for a nominal distance d between target and degrader is given by the equation:

$$d' = (d + d_{deg})\frac{1}{cos\ 27°}$$

The detectors of CLARA placed around 90° with respect to the CLARA-PRISMA symmetry axis could not be used to measure lifetimes since the Doppler shift of a γ ray emitted in flight is close to zero for such detectors. Therefore we used the 12 detectors placed at $\theta = 159.5°$ (see Fig. 3.4) with respect to the recoiling ions entering into PRISMA.

3.6 Analysis and velocity estimate

We will start by presenting the analysis for the ^{50}Ca nucleus. Fig. 3.5(a) shows the mass spectrum for Calcium nuclei as reconstructed by PRISMA. By gating on mass $A = 50$, we obtain the γ spectrum in coincidence with ^{50}Ca (in Fig. 3.5(b) we show the γ spectrum for the target-degrader distance $d = 300$ μm). The main peak at an energy of 1026 keV corresponds to the $2^+ \longrightarrow 0^+$ transition. In such spectrum, and in those at other distances, we will measure the areas of the shifted and unshifted peaks to derive the Ratio R as defined in Equation 3.9.

To obtain the value of the lifetime τ, we need to know the average velocity β of the ions before the degrader, which is bounded to the average velocity β' of the ions that passed the degrader by Eq. 3.4. The average angle of the remaining 16 clover detectors with respect to the optical axis of PRISMA is

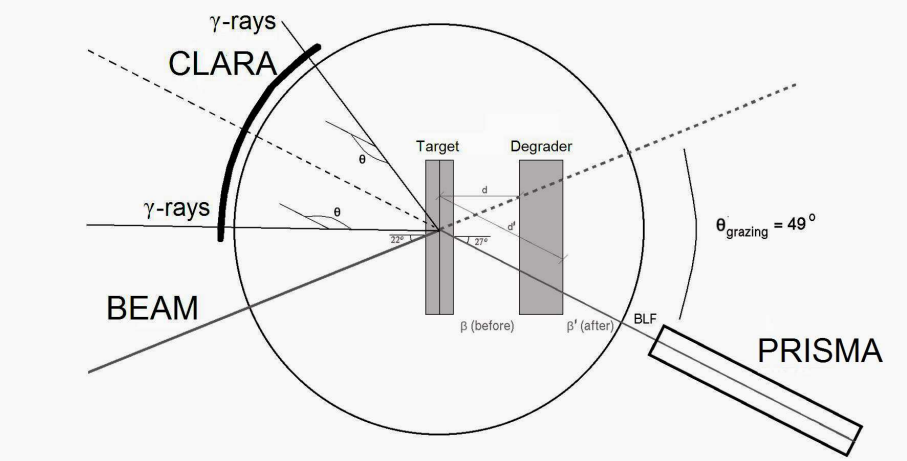

Figure 3.4: Schematic view of the reaction chamber with the plunger setup, CLARA and PRISMA spectrometers. The d' variable is called d_{eff} in the text.

$\theta = 154.2°$. Gating in the mass spectrum on $A = 50$ we obtain the distribution of β', associated to $\theta = 154.2°$, as measured event-by-event by PRISMA (Fig. 3.5(c)). The value of β' is obtained from the centroid of this distribution of the velocities measured by PRISMA and the associated error can be estimated as the σ of an approximate gaussian distribution, related to the FWHM (Full Width Half Maximum) of the peak by:

$$\sigma = \frac{FWHM}{2\sqrt{2\ln 2}} \simeq \frac{FWHM}{2.355} \tag{3.10}$$

Therefore, we obtain for β' :

$$\beta' = 0.083 \pm 0.006$$

Substituting in Eq. 3.4 to β' the value obtained before and to $E_0^{shifted}$ and E_0 the centroids of the shifted and unshifted peaks respectively of a transition in the γ spectrum, we can extract the value of β:

$$\beta = \beta' - \frac{E_0 - E_0^{shifted}}{E_0\, cos\theta} = 0.100 \pm 0.009 \tag{3.11}$$

In the same way we analyzed the data of ^{51}Sc nucleus. As we can see in Fig. 3.6(a), a gate was set on $A = 51$ in the mass spectrum and the corresponding γ spectrum obtained for $d = 300\ \mu m$ is shown in Fig. 3.6(b). The peak at 1065-keV corresponds to the $11/2^- \longrightarrow 7/2^-$ transition. Using the same method as before, we derived the value of β' as the centroid of the velocity distribution (Fig. 3.6(c)) and then β from Eq. 3.4.

We obtain:

$$\beta' = 0.080 \pm 0.008$$

$$\beta = 0.100 \pm 0.011$$

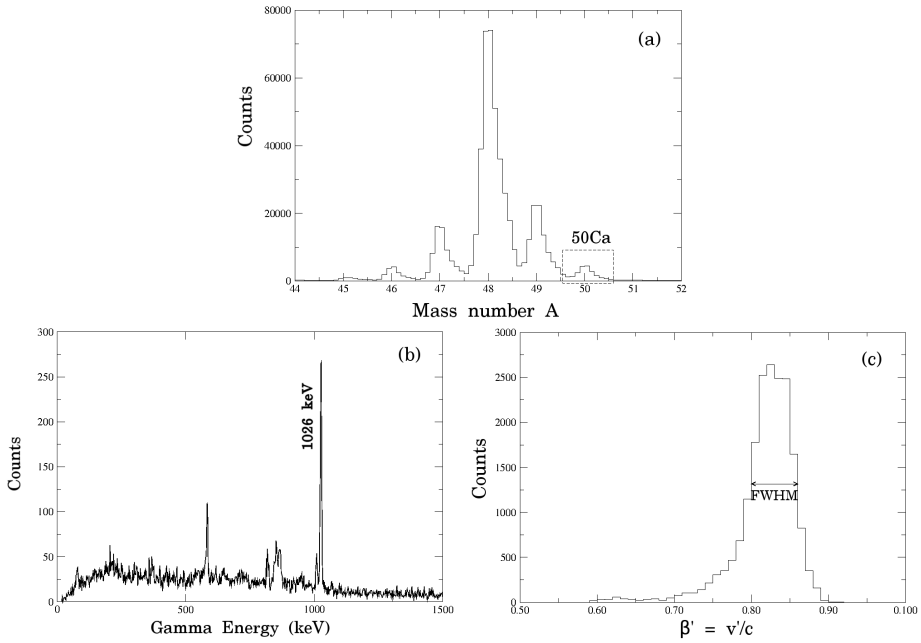

Figure 3.5: Mass spectrum of Calcium isotopes with the gating conditions on ^{50}Ca shown (a). The Doppler-corrected γ spectrum of ^{50}Ca for $d = 300\,\mu m$ (b). The distribution of the velocity β' of the ions after the degrader as measured event-by-event by PRISMA for ^{50}Ca (c).

3.7 Lifetime of the first excited state in ^{50}Ca

The first two states of the ^{50}Ca nucleus are reported in Fig. 3.7. The transition highlighted in figure 3.5(b) de-excites the first excited (2^+) level at 1026-keV.

In Fig. 3.8 the γ spectra for different distances between target and degrader are shown.

The areas of the shifted and the unshifted peaks were determined through a gaussian fit; the Ratio R was calculated according to Eq. 3.9 and the absolute error is given by:

$$\sigma_R = \sqrt{\left(\frac{I_s}{(I_s + I_u)^2}\right)^2 \sigma_{I_s}^2 + \left(\frac{I_u}{(I_s + I_u)^2}\right)^2 \sigma_{I_u}^2} \tag{3.12}$$

The resulting values for the areas of the shifted (I_s) and unshifted (I_u) peaks as well as their ratio (R) are reported in Table 3.1.

By setting a logarithmic scale on the y-axis, the experimental data have then been fitted with the function $y = -mx$ to extract the lifetime τ (Fig. 3.9), where $m = (v\tau)^{-1}$.

The velocity is $v = 24.8 \pm 2.7\ \mu m/ps$ (see section 3.6).

The resulting lifetime is:

$$\tau = 111 \pm 12\, ps$$

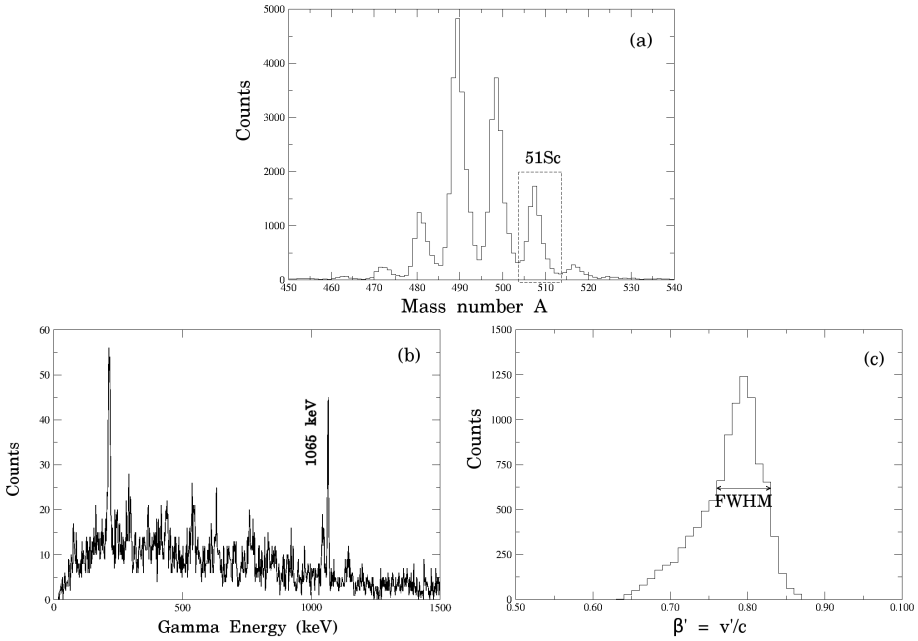

Figure 3.6: Mass spectrum of Scandium isotopes with the gating conditions on ^{51}Sc shown (a). The Doppler-corrected γ spectrum of ^{51}Sc for $d = 300\,\mu m$ (b). The distribution of the velocity β' of the ions after the degrader as measured event-by-event by PRISMA for ^{51}Sc (c).

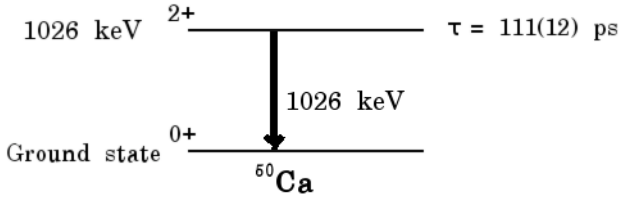

Figure 3.7: The first two states of ^{50}Ca, highlighting the transition de-exciting the first excited state.

d*(d')* (μm)	I_s	I_u	R	-ln(R)
300 *(363)*	116(20)	837(48)	0.88(0.02)	0.13(0.02)
1200 *(1418)*	258(29)	509(41)	0.66(0.03)	0.41(0.05)
2200 *(2495)*	136(13)	111(10)	0.45(0.02)	0.80(0.07)

Table 3.1: Experimental values for different target-degrader distances of the shifted peak I_s, the unshifted peak I_u and the Ratio R, with associated errors in brackets, for the 1026-keV transition.

3.8 Lifetime of the first excited state in ^{51}Sc

The first two states of the ^{51}Sc nucleus are reported in Fig. 3.10. The transition observed in Fig. 3.6(b) de-excites the first excited $(11/2^-)$ level at 1065-keV.

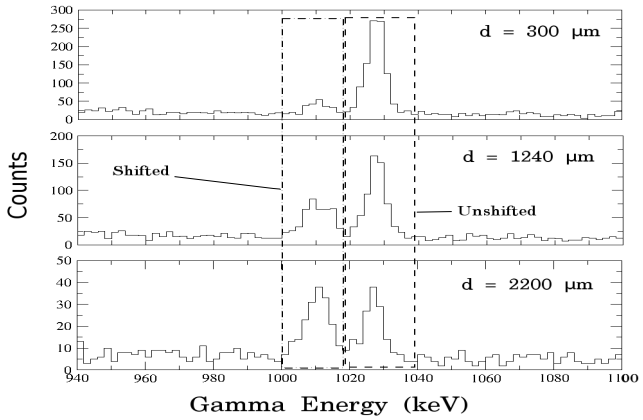

Figure 3.8: Doppler-corrected γ-ray spectra for the 1026-keV transition in ^{50}Ca for different values of the target-degrader distance d.

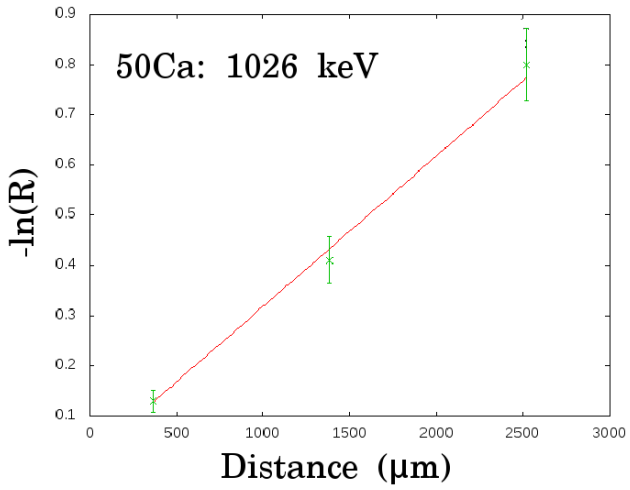

Figure 3.9: Linear fit of $-ln(R)$ as a function of the distance d_{eff} for the 1026-keV γ-ray transition.

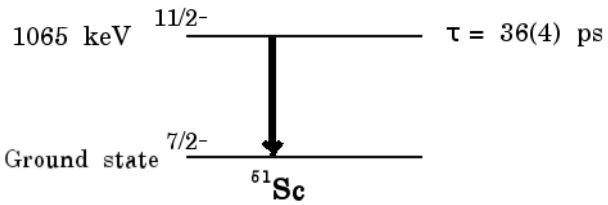

Figure 3.10: The first two states of ^{51}Sc, highlighting the transition de-exciting the first excited state.

In Fig. 3.11 the γ spectra for different distances between target and degrader

is shown.

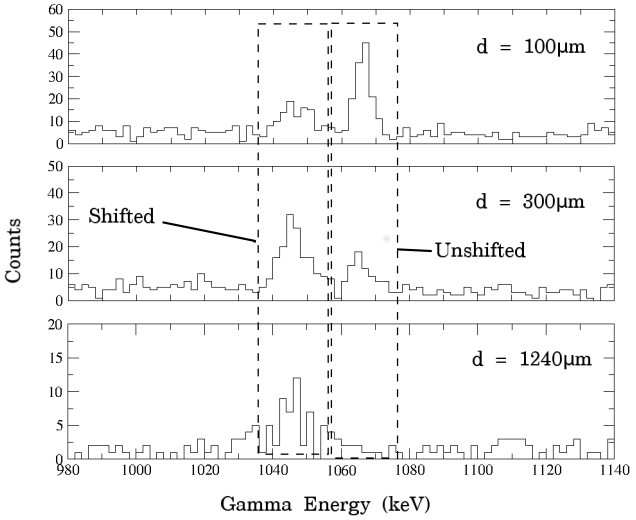

Figure 3.11: Doppler-corrected γ-ray spectra for the 1065-keV transition in ^{51}Sc for different values of the target-degrader distance d.

The resulting values for the areas of the shifted (I_s) and unshifted (I_u) peaks as well as their ratio (R) are reported in Table 3.2.

d*(d')* (μm)	I_s	I_u	R	-ln(R)
100 *(138)*	25(14)	269(31)	0.91(0.04)	0.09(0.05)
300 *(363)*	106(23)	288(40)	0.73(0.04)	0.31(0.07)
1240 *(1418)*	107(19)	44(10)	0.29(0.04)	1.23(0.20)

Table 3.2: Experimental values for different target-degrader distances of the shifted peak I_s, the unshifted peak I_u and the Ratio R, with associated errors in brackets, for the 1065 keV γ-ray transition.

By setting a logarithmic scale on the y-axis, the experimental data have been fitted with the function $y = -mx$ to extract the lifetime τ (fig. 3.12), where $m = (v\tau)^{-1}$.

The velocity is $v = 23.9 \pm 3.3\ \mu m/ps$ (see section 3.6) and therefore the resulting lifetime is:

$$\tau = 36 \pm 4\, ps$$

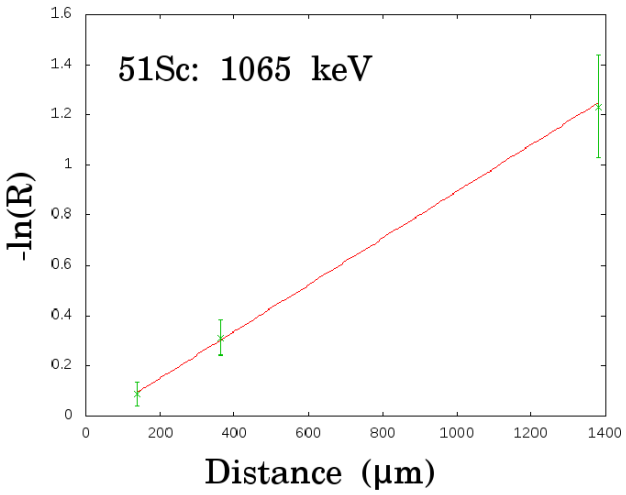

Figure 3.12: Linear fit of $-ln(R)$ as a function of the distance d_{eff} for the 1065-keV transition.

3.9 Discussion

We will now compare the transition probabilities obtained experimentally with the ones predicted theoretically. Both transitions, the one at 1026 keV of ^{50}Ca corresponding to the $2^+ \longrightarrow 0^+$ transition, and that at 1065 keV of ^{51}Sc corresponding to the $11/2^- \longrightarrow 7/2^-$ transition, are of E2 character (electric quadrupole).

The transition probability B(E2) is related to the measured lifetime of the state and to the measured energy by [13]:

$$B(E2) = \frac{1}{1.23 \cdot 10^9 E_\gamma^5 \times \tau} \tag{3.13}$$

where τ is the lifetime of the level (in seconds), E_γ is the energy of the transition (in MeV) and B(E2) is the transition probability (in $e^2 fm^4$).

By assuming a pure E2 single-particle transition, the theoretical prediction for a purely single-particle transition is given by the Weisskopf estimate [14]:

$$B(E2) = \frac{1}{4\pi} \left(\frac{3}{5}\right)^2 (1.2)^4 A^{\frac{4}{3}} \tag{3.14}$$

where A is the mass number of the nucleus and B(E2) is in $e^2 fm^4$.

Table 3.3 shows the comparison between the experimental values and the theoretical Weisskopf estimates.

By calculating the ratio between the experimental results for the B(E2) and the theoretical single-particle predictions, we obtain the transition probability in Weisskopf units: the more this ratio is closer to 1, the better the transition can be described as a pure single particle transition.

Transition	experimental B(E2) (e^2fm^4)	Weisskopf B(E2) (e^2fm^4)	Weisskopf units
^{50}Ca: 1026 keV	6.4(7)	10.9	0.6(1)
^{51}Sc: 1065 keV	20(2)	11.2	1.8(2)

Table 3.3: Experimental values, Weisskopf estimates and Weisskopf units for the transition probability B(E2) of the 1026 and 1065-keV transitions in ^{50}Ca and ^{51}Sc respectively.

As one can see, the Weisskopf units associated to both transitions are close to the unit. This allows us to conclude that both 1026- and 1065-keV transitions can be considered to have a single particle character.

Chapter 4

Isomeric states in nuclei around the doubly magic nucleus ^{208}Pb

In this chapter I will discuss the lifetime results obtained for some excited states of the ^{198}Au and ^{202}Pb nuclei which were populated through a $^{82}Se + ^{198}Pt$ multinucleon-transfer reaction. These nuclei, which are below the doubly-magic nucleus ^{208}Pb, are characterized by isomeric states as it is common for many nuclei of the region.

I will in the following explain in detail the experimental procedure, the analysis of the data, and eventually discuss the results for the states of interest.

4.1 The $^{82}Se + ^{198}Pt$ experiment

In order to populate nuclei in the region $A \approx 200$ in the neighborhood of ^{208}Pb we bombarded a ^{198}Pt target with a ^{82}Se beam at 426 MeV. The beam was provided with the *Tandem*-ALPI accelerator complex at LNL.

For the heavy-ion detection the large-acceptance magnetic spectrometer PRISMA was used . The coincident γ rays were detected by the AGATA demonstrator germanium array. Figure 4.1 shows the AGATA demonstrator (centre) together with the PRISMA spectrometer (right).

4.2 Isomeric states

It is common to call "isomers" excited nuclear states with half-lives $> 10^{-9}s$.

Different, independent phenomena can be responsible for the existence of metastable states. These are generally grouped into three categories: *spin-trap*, K- and *shape*-isomers.

For many nuclei the potential energy as a function of the deformation can have one or more minima besides the ground-state minimum. When one of

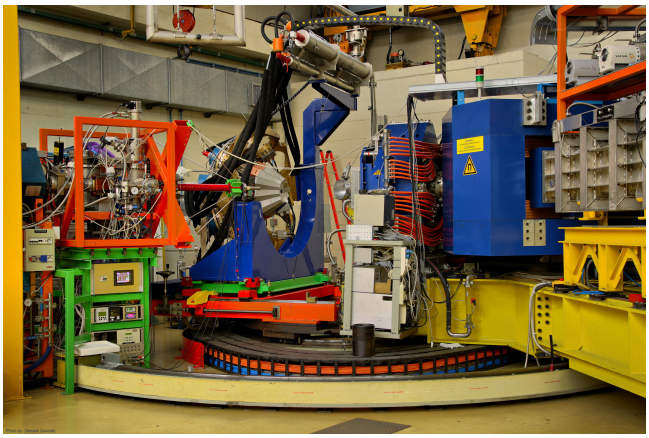

Figure 4.1: A view of AGATA demonstrator coupled to the PRISMA spectrometer.

these additional minima is sufficiently deep, then the nucleus may exist in a state corresponding to the energy and shape of this minimum. The transitions de-exciting the *shape isomer* towards states in the first minimum can be slow.

K-isomers occur in nuclei with axially symmetric deformation when there is a secondary minimum in the potential energy surface for a certain value of K, where K is the projection of the total angular momentum on the symmetry axis. Trapped in this pocket, it is difficult for the nucleus to change its spin orientation relative to the axis of symmetry. Most *K-isomers* have been found to exist in the mass A$\sim$130 and A$\sim$180 regions of the nuclear chart. In addition, transitions between the initial and final states are governed by the K-selection rule. If the difference in K-quantum number between the initial and final states, ΔK, is larger than the multipole order λ of the transition, then electromagnetic transitions are forbidden. The observation of 'K-forbidden' transitions establishes the important role of K-mixing by testing the approximate conservation of K.

If the γ-ray emission from a nuclear excited state can proceed only through a high angular-momentum transition, then the decay is slow and an isomer results. Such isomers are called *spin-trap isomers* and appear in medium to heavy nuclei near closed shells.

Another cause that may slow down the transition is a small difference in energy between the initial and the final levels involved. In Table 4.1 we show the relation between the lifetime τ, the reduced transition probability $B(\sigma\lambda)$ and the energy of the transition E for the transitions we analyzed in this work. As one can see, the lifetime depends as E_γ^3 or E_γ^5 depending on whether it is an E1 or E2. Therefore, small γ-transition energies bring long lifetimes.

Transition	Lifetime
E1 (electric dipole)	$\tau = \frac{1}{1.59 \cdot 10^{15} E_\gamma^3 B(E1)(1+\alpha)}$
E2 (electric quadrupole)	$\tau = \frac{1}{1.23 \cdot 10^{9} E_\gamma^5 B(E2)(1+\alpha)}$

Table 4.1: Relation between the lifetime τ (s), the reduced transition probability $B(\sigma\lambda)$ ($e^2 fm^{2\lambda}$) and the energy of the transition E_γ (MeV) [13]. α is the internal conversion coefficient [20].

4.3 Delayed γ-ray spectroscopy

The PRISMA spectrometer and the AGATA array are used in a coincident mode: events are collected when an ion arrives at the focal plane of PRISMA and at least one AGATA crystal is firing in coincidence. A 2.2 μs long coincidence window is used. Besides the true prompt coincidences, also random coincidences (e.g. decay of reaction products) can occur and add up to the background of the spectrum. To remove the background due to random coincidences, two equally sized gates before and after the prompt peak are placed. The background spectrum is scaled by the ratio of the sizes of the windows and subtracted from the prompt-peak spectrum.
The target-like recoils are implanted after $10 - 15$ ns from the time zero of the reaction in the target chamber. Once implanted, their γ rays can be measured if isomers with lifetimes above $5 - 10$ ns are present.
Since AGATA has no collimators and no anti-Compton shields, the γ rays can be detected with a high efficiency. The full width half maximum of the prompt peak in coincidence with the PRISMA spectrometer is around 15-18 ns depending on the reaction channel. A gate after the prompt peak allows to observe the delayed γ rays. Figure 4.2 shows the matrix of the time versus energy of the γ rays, gated on ^{80}Se, the binary partner of ^{200}Pt. The prompt peak has an arbitrary offset and is located at 2200 ns. On the right side of the peak delayed γ rays appear.

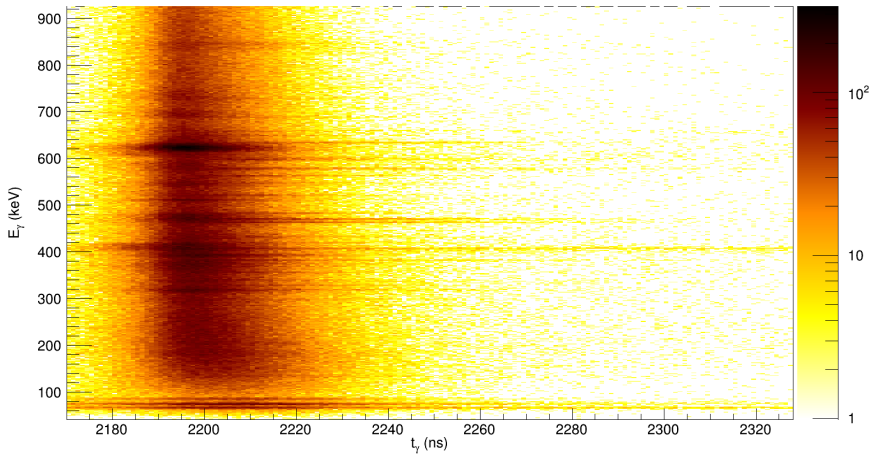

Figure 4.2: Matrix of the time of the γ ray versus the γ-ray energy gated on ^{80}Se binary partner of ^{200}Pt

Due to the evaporation of neutrons, this spectrum contains also γ rays from platinum isotopes with a lower mass. If an energy greater than the neutron separation energy is transferred to the nucleus, it might de-excite via the emission of a neutron. The emission of charged particles is hindered by the Coulomb barrier. For example, in this experiment no emission of charged particles is observed.
Figure 4.3 shows the neutron separation energy S_n for the region of the target-like fragments. The neutron separation energy drops when adding neutrons. In our experiment the excitation energy, in particular for the Pb nuclei, is higher than the neutron separation energy. Thus, it is possible that a nucleus evaporates one or more neutrons, as this is the case observed in Fig. 4.2.

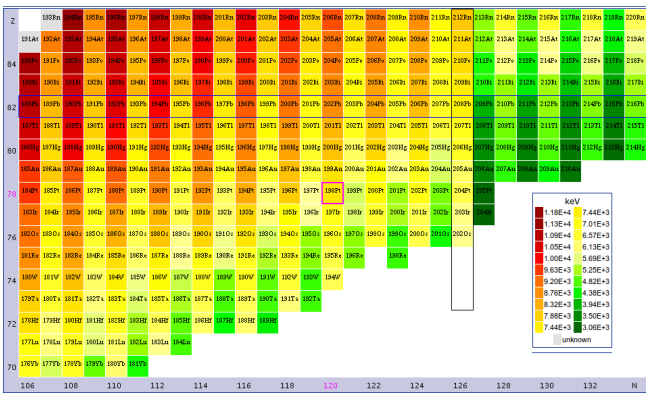

Figure 4.3: Neutron separation energy S_n for the region of the target-like fragments.

4.4 Measuring the lifetime of isomeric states

Experimental data are collected by a program in a ROOT tree with all the necessary information stored in the branches. The final spectra are then produced by correlating the observables and by projecting the variables of interest out of the tree.

For obtaining the time decay spectrum of an excited state, an Energy-Time matrix is created by correlating the corresponding observables, and a condition on the transition energy is placed. The non-correlated background is subtracted by placing equally sized background windows on an energy range lower than the transition and higher than the transition. The background is scaled with the ratio of the size of the gate on the condition to the background window size and subtracted from the transition.

The time spectrum can be fitted via an exponential decay:

$$N(t) = N_0 \, e^{-\lambda t} \tag{4.1}$$

where $\lambda = \frac{1}{\tau}$ is the decay rate and τ the lifetime of the state. The fit of an exponential decay is only valid if the fitted range is outside of the prompt peak. Due to the different time of flight of the target-like recoils, which is $t \approx 5-10ns$,

a range starting at 25 ns after the prompt peak is a safe assumption.

In many cases one has to deal with a chain of radioactive decays instead of a single one and this situation is described by successive exponential decays. For example, if we have a chain of two radioactive decays, we see that the parent level follows the simple exponential law previously described, whereas for the time evolution dN_2/dt of the daughter level we have to consider a positive contribution from the upper level and a negative contribution from the decay of the level itself, so:

$$dN_2 = \lambda_1 \cdot N_1 dt - \lambda_2 \cdot N_2 dt \tag{4.2}$$

and, taking as initial conditions $N_1(0) = N_1^0$ and $N_2(0) = N_2^0$, we obtain for the daughter level the *Bateman equation*:

$$N_2(t) = \frac{\lambda_1}{\lambda_2 - \lambda_2} N_1^0 (e^{-\lambda_1 t} - e^{-\lambda_2 t}) + N_2^0 e^{-\lambda_2 t} \tag{4.3}$$

4.5 Lifetime of the 312-keV (5^+) state in ^{198}Au

A partial level scheme of the ^{198}Au nucleus is reported in Fig. 4.4. The γ transition at 97 keV is de-exciting the level of interest.

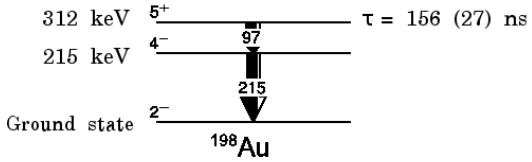

Figure 4.4: The level scheme of ^{198}Au, taken from Ref. [15].

In Fig. 4.5 we report the AGATA demonstrator efficiency curve. As one can see, the γ spectrometer, that in this experiment used a $600\,\mu m$ tin absorber, has a lower efficiency around 100 keV, while reaches its maximum around $200 - 300$ keV.

Calling τ the 312-keV (5^+) level lifetime, the 215-keV (4^-) level is known to have a lifetime $\tau_2 \ll \tau$. It means that:

$$\frac{1}{\tau} = \lambda \ll \lambda_2 = \frac{1}{\tau_2}$$

By substituting this relation in equation 4.3, we find out that, if the 215-keV (4^-) is populated by the 312-keV (5^+) one, its decay rate is the same as that of its parent level.

We thus decided to study the decay of the 215-keV (4^-) level, that will give us the same result as if we were studying the level of interest, and presents hogher statistics due to the higher γ-efficiency in this energy region of AGATA.

First of all, a spectrum to identify the γ rays was produced by creating a matrix

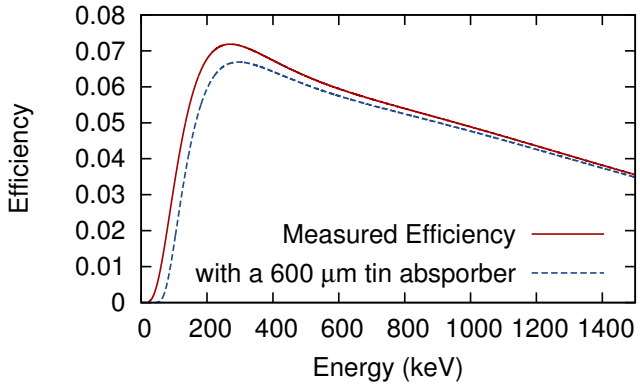

Figure 4.5: The AGATA demonstrator efficiency curve

correlating energy and time. Since our goal was to study the γ rays in coincidence with the ^{198}Au nucleus, a restriction on the mass of its binary partner ^{82}As in PRISMA was imposed.

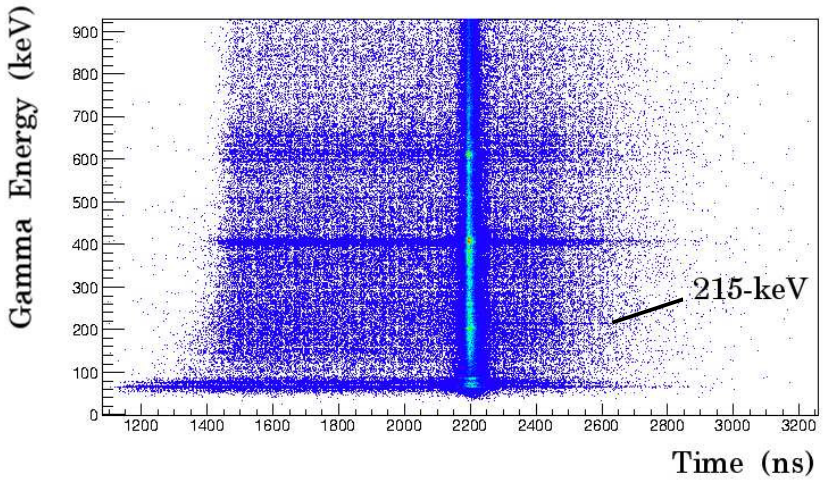

Figure 4.6: Matrix of the time of the γ ray versus the γ-ray energy gated in PRISMA on ^{82}As, binary partner of ^{198}Au. Time zero of the reaction is set at 2200 ns. The 215-keV transition de-exciting the 312-keV (5^+) isomer is highlighted.

The transition observed in Fig. 4.6 is the one de-exciting the excited level at 214-keV (4^-). By selecting the region of the delayed peaks and making a projection on the energy axis, an energy spectrum is obtained (see Fig. 4.7). A gaussian fit convoluted with a constant background is made to define the energy of the γ ray of interest.

We obtained:

$$E_\gamma = 214.9 \pm 1.7\, keV$$

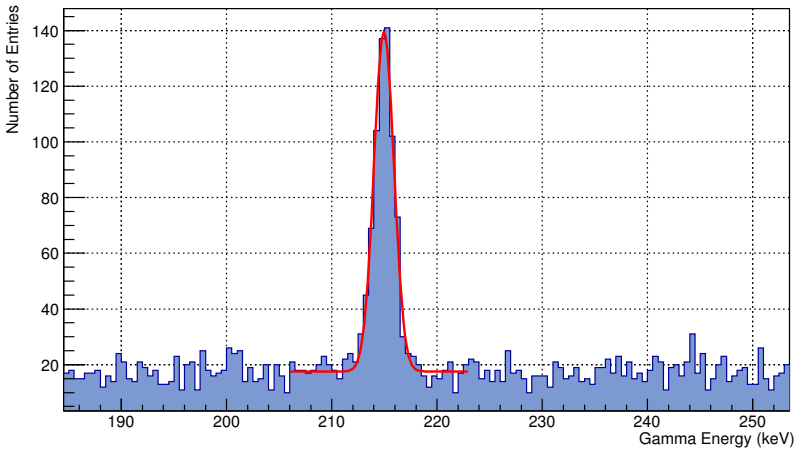

Figure 4.7: Gaussian fit of the 215-keV transition gated on the delayed region.

In order to extract the lifetime, the decay rate of the γ ray as function of the time has to be studied. By gating on the energy of the peak of interest, we project on the time axis. However, this time spectrum is affected by a non-constant background due to random coincidences. By assuming that the background in the region of interest could be well approximated by an average of the background in the adjacent upper and lower region, weighted on the numer of bins, the background is subtracted (see Fig. 4.8). After background subtraction the time spectrum obtained is shown in Fig. 4.9.

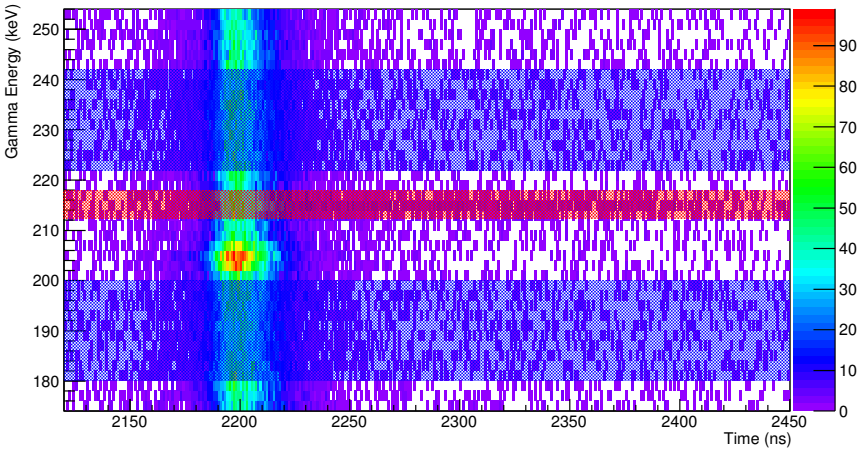

Figure 4.8: Energy gates on the 215-keV peak and its upper and lower background.

We were finally able to fit the resulting curve with the exponential law

equation, and to extract the decay constant λ. We obtained (see Fig. 4.9):

$$\lambda = 6.41602 \cdot 10^{-3} \pm 1.13015 \cdot 10^{-3}\, ns^{-1}$$

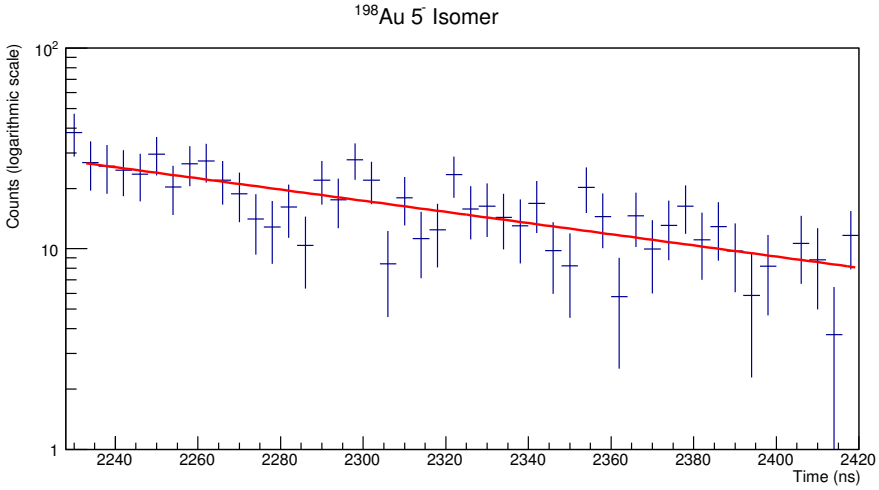

Figure 4.9: Decay curve and exponential fit of the 215-keV peak.

The lifetime of the 312-keV (5^+) state obtained in this experiment is:

$$\tau = \frac{1}{\lambda} = 156 \pm 27\, ns$$

The lifetime measured in this experiment 156 ± 27 ns is in good agreement with the known value in literature of 177 ± 9 ns [15].

4.6 Lifetimes of the $5242 + \delta$-kev (19^-) and 4091-kev (16^+) states in ^{202}Pb

A partial level scheme of the ^{202}Pb nucleus is reported in Fig. 4.10. The highlighted transitions in Fig. 4.11 are those de-exciting the 5242-keV (17^-) and 4091-keV (14^+) excited levels. The transitions of interest, which are from the $5242 + \delta$-keV (19^-) to the 5242-keV (17^-) state, and from the $4091 + \Delta$-keV (16^+) to the 4091-keV (14^+) state, have a very low energy, so far unknown, and therefore can not be detected.

The levels at 5242-keV (17^-) and 4091-keV (14^+) decay via γ-ray transitions to the $4091 + \Delta$-keV (16^+) and 3238-keV (12^+) states respectively, and have lifetimes on the order of a few picoseconds. Therefore, the λ transition probabilities associated are much bigger than those of the levels of interest. We will thus study the levels of interest in the same way we did for the ^{198}Au nucleus, id est by studying the transitions deexciting the 5242-keV (17^-) and 4091-keV (14^+) levels.

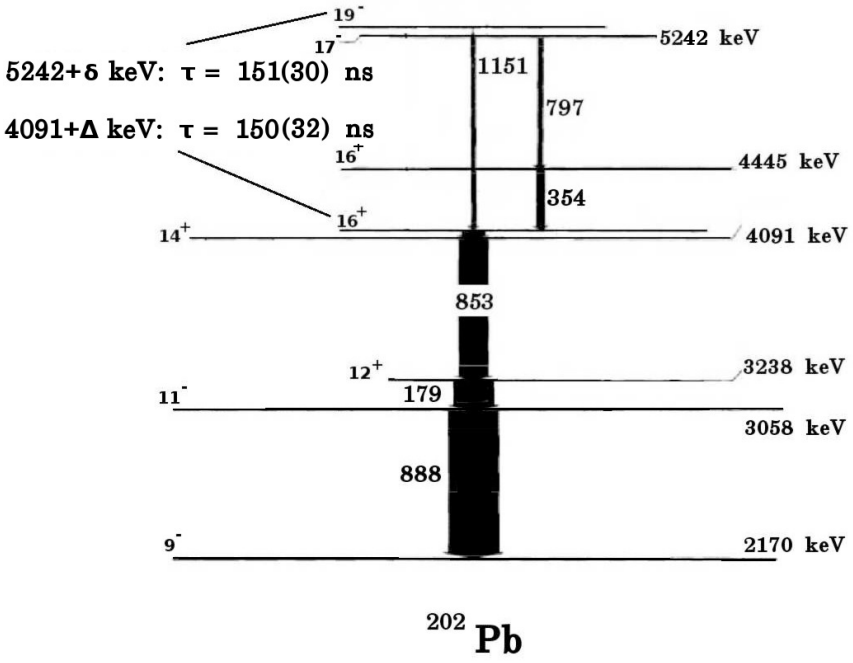

Figure 4.10: The level scheme of ^{202}Pb, adapted from Ref. [16].

Figure 4.11 shows the matrix time versus γ-ray energy without any restriction on the binary partner, but only on Z. Therefore all the γ-delayed transitions from Pb isomers are present. The labels shown correspond to ^{202}Pb.

We begin by studying the $5242 + \delta$-keV (19^-) level, focusing on the transitions deexciting the 5242-keV (17^-) level. As we can see in the level scheme (Fig. 4.10), it decays via γ emission to two different states. To extract its lifetime we can analyze both of them.

After having selected the region of the delayed peaks and made a projection on the energy axis, an energy spectrum is obtained and the γ-rays are identified by fitting them with a constant background gaussian convoluted curve, see Fig.s 4.12 and 4.13.

We obtained:

$$E_\gamma = 797 \pm 1\, keV$$

$$E_\gamma = 1151 \pm 1\, keV$$

To extract the lifetime we proceeded separately studying the two γ rays in the same way as for the ^{198}Au nucleus, and then made a weighted average of the two different results for the lifetime τ.

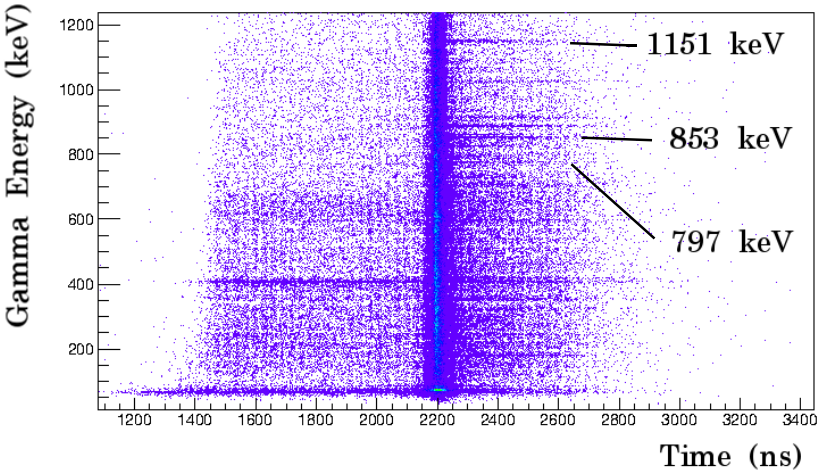

Figure 4.11: Matrix of the time of the γ-ray versus the γ-ray energy associated to all Pb nuclei. Time zero of the reaction is set at 2200 ns. The 797, 853 and 1151-keV transitions de-exciting the $5242+\delta$-kev (19^-) and $4091+\Delta$-kev (16^+) states in ^{202}Pb are shown in figure.

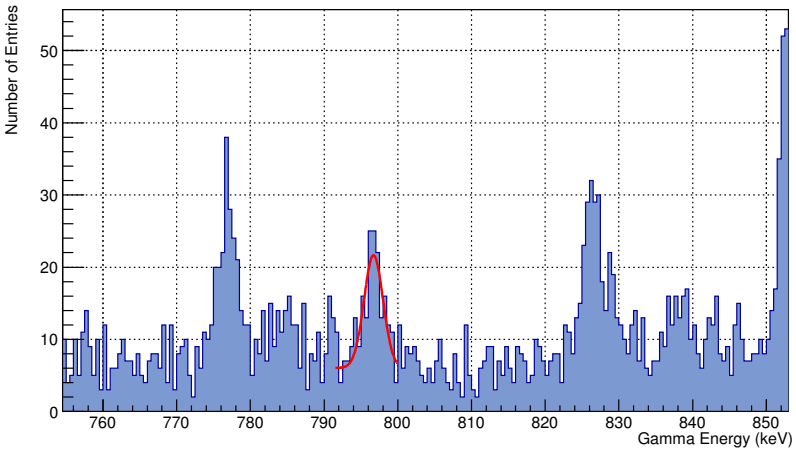

Figure 4.12: Gaussian fit of the 797-keV transition.

After having subtracted the background, we fitted the resulting curves with an exponential equation, and extracted the decay constant λ.

From the 797-keV transition (see Fig. 4.14) we obtained:

$$\lambda = 6.35826 \cdot 10^{-3} \pm 2.89758 \cdot 10^{-3}\ ns^{-1}$$

while, from the 1151-keV (see Fig. 4.15):

$$\lambda = 6.69067 \cdot 10^{-3} \pm 1.49176 \cdot 10^{-3}\ ns^{-1}$$

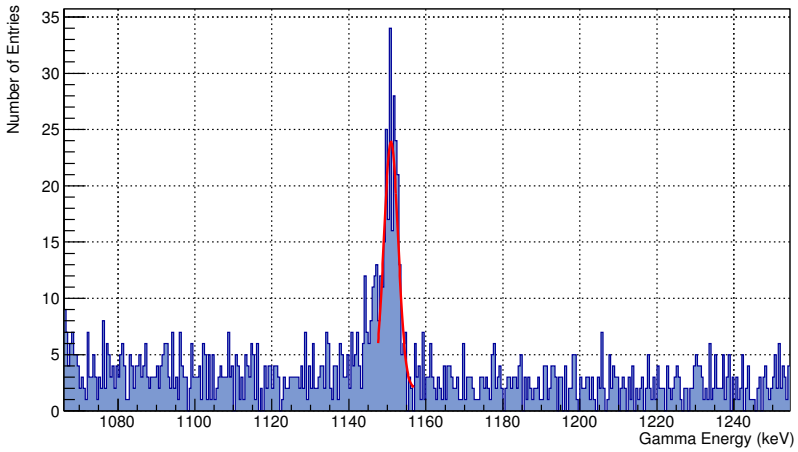

Figure 4.13: Gaussian fit of the 1151-keV transition.

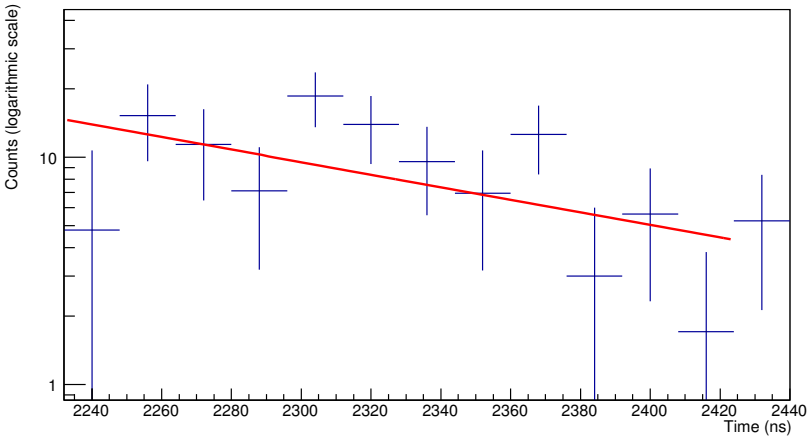

Figure 4.14: Decay curve and exponential fit for the 797-keV transition.

The 797-keV γ ray gives us, as a result:

$$\tau = \frac{1}{\lambda} = 157 \pm 72\, ns$$

while, from the 1151-keV γ ray we obtained:

$$\tau = \frac{1}{\lambda} = 149 \pm 33\, ns$$

By making a weighted average of the two results, the half life obtained for the $5242 + \delta$-keV (19^-) state is:

$$\tau = 151 \pm 30\, ns$$

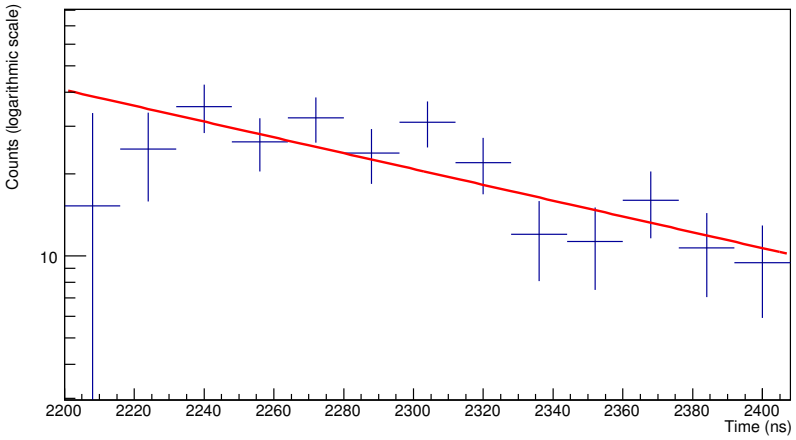

Figure 4.15: Decay curve and exponential fit for the 1151-keV transition.

The lifetime measured in this experiment 151 ± 30 ns is in good agreement with the known value in literature of 154 ± 7 ns [17].

We will now study the $4091 + \Delta$-keV (16^+) level by focusing on the transition deexciting the 4091-keV (16^+) level.

As visible in Fig. 4.10, the $4091 + \Delta$-keV (16^+) excited state is populated by the previously studied transitions, therefore when calculating the lifetime we will have to consider a fit for two consecutive decays. We started by identifying the energy of the γ transition de-exciting the 14^+ state, see Fig. 4.16.

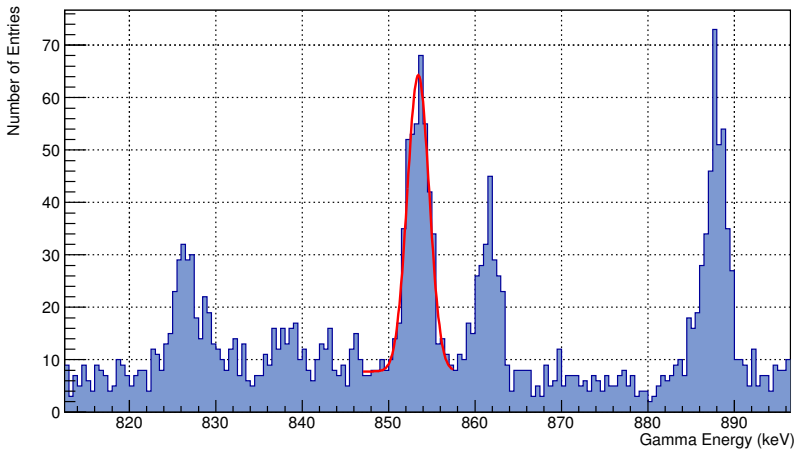

Figure 4.16: Gaussian fit of the 853-keV γ-ray transition.

We obtained:

$$E_\gamma = 853 \pm 1\, keV$$

To extract its lifetime, we proceeded in the same way as we did for the previous levels, but after having subtracted the background we fitted the final spectrum with the *Bateman equation* in Eq. 4.3.

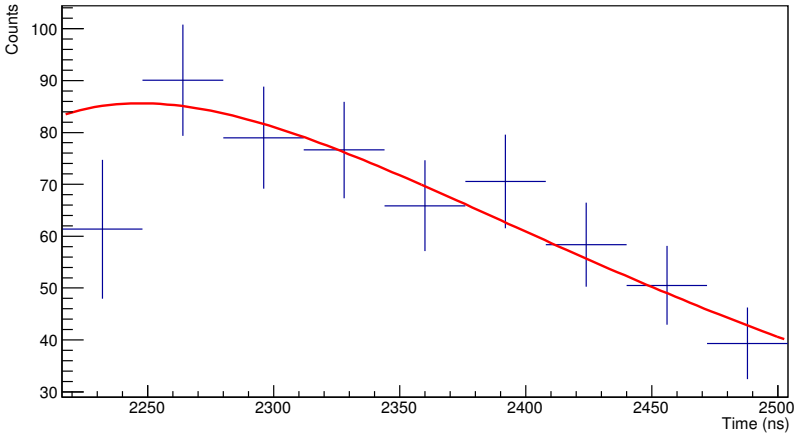

Figure 4.17: The Bateman equation fit for the 853-keV transition.

We extracted the level decay constant λ from the *Bateman equation* by fixing the λ of the $5242 + \delta$-keV (19^-) state we obtained previously. The result for the decay constant λ is:

$$\lambda = 6.86234 \cdot 10^{-3} \pm 1.54553 \cdot 10^{-3}\, ns^{-1}$$

The lifetime of the $4091 + \Delta$-keV (16^+) state obtained in this experiment is:

$$\tau = \frac{1}{\lambda} = 150 \pm\ 32 ns$$

The lifetime measured in this experiment 150 ± 32 ns is in good agreement with the known value in literature of 158 ± 7 ns [16].

4.7 Discussion

In this chapter we have analyzed data of four transitions, corresponding to the deexcitement of three isomeric levels, one in ^{198}Au and two in ^{202}Pb.

In ^{198}Au, the analysis of the 215-keV transition de-exciting the 4^- level below the 5^+ at 312-keV gave us the lifetime of the 5^+ level. In ^{202}Pb, we analyzed the 797-keV $(17^- \longrightarrow 16^+)$ and 1151-keV $(17^- \longrightarrow 16^+)$ transitions de-exciting the 5242-keV (17^-) level. Those transitions gave us the lifetime of the level of interest at $5242 + \delta$-keV (19^-), de-exciting to the (17^-) state at 5242 keV. Then

we analyzed the 853-keV ($14^+ \longrightarrow 12^+$) transition de-exciting the 4091-keV (14^+) level, giving the lifetime of the $4091 + \Delta$-keV (16^+) state.

In ^{198}Au, the 312-keV (5^+) level decays to the 215-keV (4^-) with an E1 (Electric dipole) transition.
The transition probability B(E1) is related to the measured lifetime of the state and the measured γ energy by [13]:

$$B(E1) = \frac{1}{1.59 \cdot 10^{15} E_\gamma^3 \times \tau(1+\alpha)} \tag{4.4}$$

where τ is the lifetime of the level (in seconds), E_γ is the energy of the transition (in MeV) and B(E1) is the transition probability (in e^2fm^2). The internal conversion coefficient is for this case $\alpha = 0.448$ as calculated in Ref. [19].
By assuming a pure E1 single-particle transition, the theoretical prediction for a purely single-particle transition is given by the Weisskopf estimate [14]:

$$B(E1) = \frac{1}{4\pi}\left(\frac{3}{4}\right)^2 (1.2)^2 A^{\frac{2}{3}} \tag{4.5}$$

where A is the mass number of the nucleus and B(E1) is in e^2fm^2.
Table 4.2 shows the comparison between the experimental values, the theoretical Weisskopf estimates and the transition probability in Weisskopf units.

Transition	exp. B(E1) (e^2fm^2)	Weisskopf B(E1) (e^2fm^2)	W. u.
^{198}Au: 97 keV	$(4.4 \pm 0.7) \cdot 10^{-6}$	2.2	$(2.1 \pm 0.3) \cdot 10^{-6}$

Table 4.2: Experimental values, Weisskopf estimates and Weisskopf units for the transition probability B(E1) of the 97-keV transition.

As one can see, the transition probability is much smaller of 1 W.u. A suppression factor of 10^{-6} for E1 transitions which is obtained from our data is not uncommon [18].

In ^{202}Pb the $5242 + \delta$-keV (19^-) level decays to the 5242-keV (17^-), and the $4091 + \Delta$-keV (16^+) level decays to the 4091-keV (14^+). In both cases the most probable character of the de-exciting transition is E2 (Electric quadrupole).
Since the E_γ is not known in neither of the cases it is not possible to calculate the B(E2) reduced transition probability rate. However, if one assumes as reasonable a γ-ray transition of around 40 keV, then it is possible to calculate the experimental B(E2) and compare it to the Weisskopf estimate.

The experimental value is given by [13]:

$$B^{exp}(E2) = \frac{1}{1.23 \cdot 10^9 \cdot E_\gamma^5 (1+\alpha) \cdot \tau} \tag{4.6}$$

where τ is the lifetime (in seconds) E_γ is the energy of the transition (in MeV) and α is the internal conversion coefficient.
The Weisskopf estimate for the B(E2) of a pure single-particle transition is given by Eq. 3.14. The results are shown in table 4.3.

Transition	$B^{exp}(E2)(e^2fm^4)$	$B^W(E2)(e^2fm^4)$
^{202}Pb: $19^- \rightarrow 17^-$	94(18)	70.4
^{202}Pb: $16^+ \rightarrow 14^+$	102(22)	70.4

Table 4.3: Experimental results and Weisskopf estimates for the B(E2) of the transitions de-exciting the levels of interest in ^{202}Pb.

For both transitions, the internal conversion coefficient is $\alpha = 477$ as calculated in Ref. [19].
The B(E2) reduced transition probability rate is close to the Weisskopf estimate, pointing out to a single particle character for the states discussed.

Chapter 5

Summary and conclusions

In this work the lifetimes of excited states produced in two different experiments have been studied.

In the first part the first excited states of the ^{50}Ca and ^{51}Sc nuclei have been discussed. The two nuclei were produced by a multi-nucleon transfer reaction between an incident beam of ^{48}Ca, at a bombarding energy of 310 MeV, and a ^{208}Pb target.

In the second part the isomeric states in the ^{198}Au and ^{202}Pb nuclei were discussed. In this case the nuclei of interest were provided via a multi-nucleon transfer reaction between an incident beam of ^{82}Se, at a bombarding energy of 426 MeV, and a ^{198}Pt target.

In the first experiment, lifetimes have been measured using the RDDS method. This method consists in placing, at a known and variable distance after the target, an energy degrader and then measuring, as function of such distance, the number of γ-rays emitted before and after the degrader by the recoiling ions, whose mass and atomic number are then identified by the PRISMA spectrometer. Depending on whether a γ-ray, de-exciting a particular state, is emitted before or after the degrader, it will exhibit different Doppler shifts. As a consequence, for each transition, the γ spectra show two peaks. The relative intensities of the peak areas as a function of the target-degrader distance determines the lifetime of the state of interest.

The ^{50}Ca nucleus studied in this thesis has two neutrons more than the doubly-magic nucleus ^{48}Ca, while ^{51}Sc has one proton and two neutrons more than ^{48}Ca. The knowledge of the lifetimes of their excited states is a stringent test for theoretical Shell Model calculations of nuclei around the double shell-closure ($Z = 20$, $N = 28$) of ^{48}Ca.

We analyzed the γ-ray transitions of 1026 keV for ^{50}Ca and 1065 keV for ^{51}Sc. From this analysis we obtained the lifetimes for the first excited levels of the two nuclei, at 1026 keV (2^+) and 1065 keV ($11/2^-$) respectively.

^{50}Ca

For the ^{50}Ca nucleus we obtained for the first excited state (2^+) at 1026 keV a lifetime of $\tau = 111 \pm 12\, ps$.

^{51}Sc

For the ^{51}Sc nucleus we obtained for the first excited state ($11/2^-$) at 1065 keV

a lifetime of $\tau = 36 \pm 4\, ps$.
The comparison between the experimental B(E2) transition probabilities and the Weisskopf estimates for a single-particle transition shows that both transitions in ^{50}Ca and ^{51}Sc can be considered as pure E2 single-particle transitions.

In the second experiment, lifetimes of isomeric states have been measured by observing the exponential decay of γ rays emitted by the recoiling ions once implanted in the chamber.

The ^{198}Au and ^{202}Pb nuclei studied in this thesis are few nucleons below the doubly-magic nucleus ^{208}Pb ($Z = 82$, $N = 126$). We analyzed the γ-ray transitions of 215 keV for ^{198}Au and 796, 1151 and 853 keV for ^{202}Pb. From this analysis we extracted the lifetimes for the 312-keV (5^+) level of ^{198}Au and the $5242 + \delta$-keV (19^-) and $4091 + \Delta$-keV (16^+) levels of ^{202}Pb.

^{198}Au

For the ^{198}Au nucleus we obtained the lifetime of the 312-keV (5^+) state, $\tau = 156 \pm 27\, ns$.
The comparison between the experimental B(E1) transition probability and the Weisskopf estimate for a single-particle transition shows us that the transition presents a typical suppression factor of 10^{-6}.

^{202}Pb

For the ^{202}Pb nucleus we obtained for the $5242 + \delta$-keV (19^-) and $4091 + \Delta$-keV (16^+) lifetimes of: $\tau = 151 \pm 30\, ns$ and $\tau = 150 \pm 32\, ns$, respectively.
The comparison between the experimental B(E2) transition probability and the Weisskopf estimate for a single-particle transition shows that also in this case the isomers can be described as single-particle states.

Bibliography

[1] A. Stefanini, Nucl. Phys. A 701, 217c (2002).

[2] A. Gadea et al., Eur. Phys. J. A 20, 193 (2003).

[3] R. Krucken et al., Phys. Rev. C 64, 017305 (2001).

[4] A. Dewald et al., Prog. Part. Phys. and Nucl. Phys. 67, 786 (2012).

[5] A. Gadea et al., Annual Report 2006 (INFN-LNL-217(2007)), pag 240 (2003).

[6] S. Akkoyun et al., Nucl. Instr. and Meth. 668, 26 (2012)

[7] A. Gadea et al., Nucl. Instr. and Meth. 654, 88 (2011)

[8] R. Broda et al., J. Phys. G 32, R151 (2006).

[9] J.J. Valiente-Dobòn et al., Phy. Rev. Lett. 102, 242502 (2009).

[10] A. Gadea et al., Acta Phys. Pol. B 38, 1311 (2007).

[11] V. Barone, Relativita , Bollati Boringhieri, Torino, 2004, pp. 82-86.

[12] K. S. Krane, Introductory Nuclear Physics, Wiley & Sons, 1987, pp. 160-173.

[13] H. Morinaga and T. Yamazaki, In-beam gamma-ray spectroscopy, North Holland Publishing Company, Oxford, 1976, pp. 54.

[14] J.M. Blatt and V.F. Weisskopf, Theoretical Nuclear Physics, John Wiley and Sons Inc., New York, 1952.

[15] J. C. Cunnan and J.Daly, Phys. Rev. C, 4 (1972)

[16] Nuclear Physics A458, 225 (1986)

[17] Nuclear Physics A475, 338 (1987)

[18] Journal of NUCLEAR SCIENCE and TECHNOLOGY, Supplement 2, p. 450-454 (August 2002)

[19] bricc.anu.edu.au/index.php

[20] C. M. Perchisat Rev. Mod. Phys. 38 (1966) 41